Am J Physiol Heart Circ Physiol 319: H507–H518, 2020.
First published July 24, 2020; doi:10.1152/ajpheart.00175.2020.

RESEARCH ARTICLE | *Vascular Biology and Microcirculation*

TRPV4 channels' dominant role in the temperature modulation of intrinsic contractility and lymph flow of rat diaphragmatic lymphatics

Eleonora Solari, Cristiana Marcozzi, Michela Bistoletti, Andreina Baj, Cristina Giaroni, Daniela Negrini, and Andrea Moriondo

Department of Medicine and Surgery, University of Insubria, Varese, Italy

Submitted 11 March 2020; accepted in final form 20 July 2020

Solari E, Marcozzi C, Bistoletti M, Baj A, Giaroni C, Negrini D, Moriondo A. TRPV4 channels' dominant role in the temperature modulation of intrinsic contractility and lymph flow of rat diaphragmatic lymphatics. *Am J Physiol Heart Circ Physiol* 319: H507–H518, 2020. First published July 24, 2020; doi:10.1152/ajpheart.00175.2020.—The lymphatic system drains and propels lymph by extrinsic and intrinsic mechanisms. Intrinsic propulsion depends upon spontaneous rhythmic contractions of lymphatic muscles in the vessel walls and is critically affected by changes in the surrounding tissue like osmolarity and temperature. Lymphatics of the diaphragm display a steep change in contraction frequency in response to changes in temperature, and this, in turn, affects lymph flow. In the present work, we demonstrated in an ex vivo diaphragmatic tissue rat model that diaphragmatic lymphatics express transient receptor potential channels of the vanilloid 4 subfamily (TRPV4) and that their blockade by both the nonselective antagonist Ruthenium Red and the selective antagonist HC-067047 abolished the response of lymphatics to temperature changes. Moreover, the selective activation of TRPV4 channels by means of GSK1016790A mirrored the behavior of vessels exposed to increasing temperatures, pointing out the critical role played by these channels in sensing the temperature of the lymphatic vessels' environment and thus inducing a change in contraction frequency and lymph flow.

NEW & NOTEWORTHY The present work addresses the putative receptor system that enables diaphragmatic lymphatics to change intrinsic contraction frequency and thus lymph flow according to the changes in temperature of the surrounding environment, showing that this role can be sustained by TRPV4 channels alone.

intrinsic contractility; lymph flow; TRPV channels

INTRODUCTION

Lymphatic vessels drain fluid, macromolecules, and cells from the interstitial space (37, 53), thus guaranteeing fluid balance and, when referred to the pleural space, the proper lung-chest wall coupling (15, 23). Lymph formation and propulsion occur by exploiting two different propulsive mechanisms (5, 6, 30, 31). One of them, the so-called intrinsic mechanism, relies on rhythmical contractions of a layer of lymphatic muscle (LM) cells around the lymphatic endothelium of collecting lymphatics (7, 28, 35, 49, 51, 55). The spontaneous contractions of lymphatic vessels are most likely due to either spontaneous transient depolarizations (STDs), as in mesenteric lymphatics (47, 50), or to I_f-like currents typical of cardiac pacemaker cells of the sinoatrial node mediated by HCN channels, as reported both in mesenteric and diaphragmatic lymphatics (19, 29). The other mechanism, called extrinsic, depends upon mechanical stresses arising in the surrounding tissues and transmitted to the lymphatic vessels, such as those occurring during cardiogenic activity (32), respiratory movements (24), or the contraction of skeletal muscle fibers (22, 26, 36). Depending on the location of lymphatic vessels in different body regions, the two propulsive mechanisms can sometimes coexist, such as occurs in the diaphragm (27). Unlike the response observed in the medial central diaphragm, lymphatic vessels located at the muscle periphery of diaphragm display a complex pattern of spontaneous intrinsic contractions (25). Those lymphatics are located in the body thermal core and display a greater variation of intrinsic contraction frequency (f_c) in response to temperature changes in the 33–40°C range compared with lymphatics located outside the thermal core, such as those found in skin (42). This steeper response could be due to temperature-sensitive ionic channels of the transient receptor potential cation channels family (TRP).

TRP channels of the vanilloid subfamily comprise six members of cation channels (V1–V6) (17), four of which serve as temperature sensors in different tissues (1, 3). Members of the V1, V3, and V4 subfamilies possess temperature ranges of activation that are compatible with the physiological temperature of the body thermal core and have a high reaction rate increase for every 10° rise in temperature (Q_{10} value) (11). Thus, they are likely candidates to sense temperature changes in diaphragmatic lymphatics.

Indeed, apart from febrile states, where temperature increase and later decrease can be of 1–3° at worst, temperature of muscle-associated lymphatic vessels is subjected to the heat generated by their activity, and, for those belonging to the muscles of the limbs, it can also decrease on the basis of the environment temperature and the necessity to preserve the body core temperature. Core temperature itself is said to be held constant, but indeed, during exercise it may vary from fraction of degrees or 2 to 3° due to the heat produced by muscles in combination with the capacity of the environment to support heat dispersion from the body (33, 44, 46). In rats, the core temperature is subjected to higher temperature variations exacerbated by the less efficient heat dissipation mechanism when ambient temperature increases above ~32°C, and also, circadian rhythms cause core temperature to vary in a range of ±1°C (34, 39).

In the present work, we present gene expression and functional and immunohistochemical results obtained in an ex vivo diaphragmatic tissue rat model to support the hypothesis that

Correspondence: A. Moriondo (andrea.moriondo@uninsubria.it).

TRPV4 channels may be the predominant receptors involved in diaphragmatic lymphatic vessels' regulation of intrinsic frequency, and thus the lymph flow (J_{lymph}), in response to thermal changes in the surrounding tissue.

MATERIALS AND METHODS

Surgical procedures and in vivo protocol. The whole procedure was approved by the Animal Care and Use Ethics Committee of the University of Insubria (OPBA) and by the Italian Ministry of Health in accordance of the Italian D.Lgs 26/2014 (protocol 400/2015-PR). Wistar rats coming from our in-house colony were housed in groups of two to three littermates in standard plastic cages (Tecniplast SpA; Buguggiate, Varese, Italy), with ad libitum access to pellet food (standard diet) and water in a 12-h:12-h light-dark cycle.

Adult Wistar rats (both sexes, $n = 21$; mean body weight = 348 ± 28 g) were deeply anesthetized by an intraperitoneal injection of a ketamine (75 mg/kg body wt, Lobotor; ACME S.r.l.) and medetomidine (0.5 mg/kg body wt, Domitor; Pfizer) cocktail in saline solution. An additional half bolus was administered after 1 h while the appropriate level of anesthesia continuously checked, assessed by the absence of the noxious plantar reflex of the hind paw. In vivo fluorescent staining of the pleural diaphragmatic lymphatic network was performed as previously described (43). Briefly, 0.8 mL of 2% 250-kDa FITC-conjugated dextrans (Ex/Em 505/515, FD250S; Merck) in saline solution was intraperitoneally administered to deeply anesthetized animals by using a stainless-steel injecting cannula (outer diameter ~0.8 mm) carefully inserted into the peritoneal cavity and positioned into the subdiaphragmatic region. Dextrans or other nontoxic high MW molecules are a standard staining medium for lymphatic vessels since they can only be drained by lymphatic vessels due to the nonselectivity of the initial lymphatic vessels wall. By contrast, blood capillaries are almost impermeant to proteins larger than 70 kDa due to their 0.8 reflection coefficient and do not represent a draining route for FITC-dextrans injected into the interstitium or serosal cavities. Animals were then placed on a warmed (37°C) pad and allowed to spontaneously breathe for 1 h to let diaphragmatic lymphatics drain the fluorescent tracer. At the end of the loading procedure, animals were tracheotomized, and a T-shaped cannula was inserted into the trachea; then they were paralyzed with a single bolus of 2 mg/mL pancuronium bromide (P1918; Merck) in saline solution administered through the jugular vein and mechanically ventilated (Inspira; Harvard Apparatus) with room air at a tidal volume and respiratory rate automatically set by the instrument based on animals' body weight according to the internal parameter table programmed in the instrument firmware by the manufacturer (page 17 of the Inspira User Manual; Harvard Apparatus) and derived from published normal values for rats. The chest wall was then opened to expose the pleural diaphragmatic surface, and FITC-fluorescent filled lymphatic vessels were visualized under a stereomicroscope (SV11, lens ×1; Zeiss) equipped with a LED epi-illuminator (custom made from Luxeonstar high-intensity LEDs; Luxeon Star Leds), with care taken to avoid tissue dehydration through periodical rinsing of the exposed diaphragm with a flush of saline heated at 37°C.

Spontaneous contracting lymphatic vessels, typically located at the muscular diaphragmatic periphery, were video recorded in vivo at 10 fps for ≥5 min using a charge-coupled device (CCD) camera (Orca ER; Hamamatsu) connected to a PC running SimplePCI Software (Hamamatsu). From each animal, up to four or five diaphragmatic tissue specimens containing intrinsic contracting lymphatics were carefully excised from the costal margin to the central tendon (20). These were subsequently used for the ex vivo experiments and placed in petri dishes containing HEPES-buffered Tyrode's solution [119 Mm NaCl, S7653; 5 mM KCl, P9541; 25 mM HEPES buffer, H3375; 2 mM $CaCl_2$, 21115; 2 mM $MgCl_2$, 63069; 33 mM D-glucose, G5767; all products from Merck, pH = 7.4; *Cold Spring Harbor Protocols* (11a)] and kept at 4°C until being used. Immediately after the diaphragmatic tissue excision, animals were euthanized by an anesthetic overdose injection (375 mg/kg ketamine and 2.5 mg/kg medetomidine).

After excision, diaphragmatic tissue specimens were pinned down to the bottom of a perfusion chamber (RC-27D; Warner Instruments) filled with HEPES buffer-Tyrode's solution equilibrated with 21% O_2. The same geometry that lymphatic vessels displayed during in vivo video recordings was maintained to avoid any mechanical stress that could induce possible artifacts in spontaneous activity of lymphatic vessel tracts. Specimens of contracting and noncontracting lymphatic vessels and dorsal root ganglions (DRGs) were taken from six randomly chosen animals and processed for RNA extraction and quantitative real-time PCR assay.

Tissue preparation for RNA extraction and quantitative real-time PCR assay. The perfusion chamber holding the excised diaphragmatic specimen was placed on a custom-made three-dimensional (3D) printed support under the SV11 stereomicroscope. The tissue temperature in the perfusion chamber was continuously monitored by an implantable T thermocouple (Cole-Palmer) and maintained at 37.0 ± 0.1°C with a PID thermostat (ITC100-VH, Inkbird, PRC), piloting a resistive load embodied into the recording chamber. Spontaneous contracting lymphatics were video recorded ex vivo for 1 min using the CCD camera, and then video data were converted to avi and contracting sites highlighted using the "Standard Deviation Function" (41) of ImageJ Software (National Institutes of Health; https://imagej.nih.gov/ij/; see Ref. 38). From each animal, *1*) lymphatic segments displaying spontaneous contractions and *2*) lymphatic segments of comparable diameter not displaying intrinsic contractility were carefully dissected from the surrounding diaphragmatic tissue and immediately frozen in dry ice, with two lymphatic sample pools obtained to proceed with separate total RNA extraction ($n = 6$ samples each).

Total RNA extraction from lymphatic vessels was performed using *Quick*-RNA MicroPrep (R1050, Zymo Research, supplied by Euro-Clone), following the manufacturer instructions. cDNA was then generated by using the High Capacity cDNA Reverse Transcription Kit (4368814; ThermoFisher) from 100 ng of total RNA, and real-time PCR was performed on an ABI Prism 7000 instrument (Applied Biosystems, Foster City, CA) according to the procedure described in Ref. 4. Specific primers were designed using CLC Main workbench software (Qiagen), as reported in Table 1, and used at a final concentration of 500 nM to have a similar amplicon size and similar amplification efficiency as required for applying the $2^{-\Delta\Delta C_T}$ method (4).

Table 1. *Oligonucleotides used in real-time PCR experiments*

Oligo Name	Sequence (5′-3′)
Prox1	
Forward	AAACGACTTTGAGGTTCCAGAGA
Reverse	CCGCGATGATGGCATTG
LMC α-actin	
Forward	CAGAAGGAGATCACAGCCCTC
Reverse	CCGCCGATCCAGACAGAAT
β-Actin	
Forward	GACAGGATGCAGAAGGAGATTACTG
Reverse	CTCAGGAGGAGCAATGATCTTGAT
TRPV1	
Forward	ATGTGGCTTCCATGGTGTTCTC
Reverse	GAACATAAACCGGCACAGGTCTC
TRPV3	
Forward	TTATCTGGGCCATGTGCATCTC
Reverse	GGCATCTGACAGGATGGACTGA
TRPV4	
Forward	ACCAGCAAGGTTATGCTCCC
Reverse	CCAAGCCTGGGCCATTGAC

LMC α-actin, lymphatic muscle α-actin; TPRV1, -3, and -4, transient receptor potential vanilloid 1, 3, and 4, respectively.

For all genes, data were normalized on β-actin and target gene expression. TRPV mRNA levels in diaphragmatic lymphatics were further normalized on the values obtained in DRGs. For each sample, measurements were performed in duplicate.

Gene expression was performed for the lymphatic endothelium marker Prox1 and the lymphatic muscle α-actin (LMC α-actin) to confirm the lymphatic nature of the dissected tissue and the presence of lymphatic muscle in the samples for β-actin and for three transient receptor potential (TRP) channels of the Vanilloid family, TRPV1, TRPV3, and TRPV4, chosen upon their temperature range of activity.

Ex vivo functional analysis. Excised specimens lodged in the perfusion chamber were placed onto the stage of an upright fluorescent microscope (BX51WI; Olympus) equipped with an epi-fluorescence ×4 Olympus Plan APO dry objective (numerical aperture = 0.13) and with a black and white Watec camera (WAT-902H; Sicom snc) connected to a PC running VirtualDub software (http://www.virtualdub.org/), allowing 25 fps video recordings. Tissue temperature was continuously monitored and recorded by means of the implantable T thermocouple, which was placed as close as possible to the contracting tract and maintained at ± 0.1°C of the desired temperature with the ITC100-VH PID thermostat.

Four different sets of functional experiments were randomly performed on contracting diaphragmatic lymphatics while the increasing temperature test was performed from 35 to 39°C (see Table 2). To avoid possible artifacts due to repeated tests, only one spontaneous contracting vessel was video recorded for each diaphragmatic specimen, and a single condition at a time was tested.

In the control group (see Table 2), the temperature was raised from the initial temperature of the perfusion chamber set up (~20°C) to a stable temperature of 35°C, and then spontaneous contractions of FITC-filled lymphatic vessels were video recorded for 5 min in HEPES buffer-Tyrode's solution (baseline conditions). Afterward, temperature was increased up to 39°C in +0.5°C steps, maintaining the new thermal condition for ≥2 min to allow the whole diaphragmatic tissue to reach and maintain the same temperature value.

For RuR_{10} and RUR_{20} experiments (see Table 2), after 3-min baseline acclimation at 35°C in HEPES-buffer Tyrode's solution, lymphatic vessels were challenged with the nonselective TRPV1–6 channel antagonist Ruthenium Red (RuR; 10 and 20 μM, 557450; Merck; groups RuR_{10} and RuR_{20}, Table 2) at 35°C for 5 min, with lymphatic vessels' activity always video recorded. The temperature was successively incremented from 35 to 39°C in steps of +0.5°C, maintaining the temperature constantly between successive steps for ≥2 min.

In the $HC_{2.5}$ and HC_5 groups (see Table 2), lymphatic vessels were challenged with the selective TRPV4 channel blocker HC-067047 (HC, 2.5 and 5 μM, SML0143; Merck; groups $HC_{2.5}$ and HC_5; Table 2), while the same experimental procedure used in RuR groups was performed. HC-067047 was dissolved in DMSO (dimethyl sulfoxide; 41639; Merck) to prepare stock solution, and aliquots were stored at −20°C until use. Aliquots were diluted in HEPES buffer-Tyrode's solution to achieve final concentration.

Table 2. *Summary of groups used in functional experiments*

Experimental Group	Drug	Temperature
Control	None	35–39°C in +0.5 increments
RuR	Ruthenium Red	35–39°C in +0.5 increments
RuR_{10}	10 μM	
RuR_{20}	20 μM	
HC	HC-067047	35–39°C in +0.5 increments
$HC_{2.5}$	2.5 μM	
HC_5	5 μM	
$DMSO_{0.1\%}$	Dimethyl sulfoxide, 0.1%	35–39°C in +0.5 increments
GSK101	GSK1016790A, 50–350 nM	35°C constant
$DMSO_{0.01\%}$	Dimethyl sulfoxide, 0.01%	35°C constant

In the $DMSO_{0.1\%}$ group, the possible effect caused by vehicle alone (0.1% DMSO in HEPES buffer-Tyrode's solution) was tested on another set of lymphatic vessels with the same experimental paradigm (Table 2).

Each set of experiments (control, RuR, HC, and $DMSO_{0.1\%}$ groups) was performed with +0.5°C temperature increments, thus avoiding possible artifacts due to tissue preconditioning induced by repeated temperature changes.

In group GSK101 (see Table 2), lymphatic vessels were video recorded for 3 min at 35°C and then, maintaining the same temperature (35.0 ± 0.1°C over the entire experiment), exposed to increasing concentrations of the specific TRPV4 channel agonist GSK1016790A (GSK101, 10–350 nM, G0798; Merck) in HEPES buffer-Tyrode's solution for 7 min for each dose. GSK1016790A was dissolved in DMSO to prepare stock solutions, and aliquots, diluted in HEPES buffer-Tyrode's solution to achieve the desired concentration, were stored at −20°C until use.

In the $DMSO_{0.01\%}$ group (see Table 2), vehicle controls (0.01% DMSO maximum concentration in HEPES buffer-Tyrode's solution) were performed by using the same protocol for GSK101 experiments.

Whole mount immunostaining and image acquisition. Immediately after dissection, diaphragmatic tissue specimens containing FITC-filled lymphatic vessels were fixed with 4% paraformaldehyde (158127; Merck) in PBS at room temperature for 45 min and then rinsed in PBS and permeabilized with 100% ice-cold methanol and subsequently with 0.5% Triton X-100 (Merck) in PBS. Thereafter, tissue samples were incubated with blocking solution (1% BSA, 5% goat serum in PBS) for 1 h at room temperature and then with anti-TRPV4 primary antibody [1:60; anti-TRPV4 (extracellular) antibody, ACC-124; Alomone Laboratories] (8, 40) overnight at 4°C. After washes in PBS, specimens were incubated with a secondary goat anti-rabbit antibody conjugated with Texas Red (1:100, sc-2780; Santa Cruz Biotechnology) for 2 h at room temperature and then rinsed in PBS. Overnight incubation with an anti-smooth muscle actin primary antibody [1:50; Actin Alpha 2 Smooth Muscle Antibody (1A4), NB600-536 Novus Biologicals] at 4°C was then followed by rinses in PBS and a 2-h incubation with a secondary goat anti-mouse antibody conjugated to Alexa Fluor 647 (1:100, goat anti-mouse IgG2a; Molecular Probes) at room temperature. Eventually, tissue samples were rinsed in PBS and mounted onto glass coverslips with Fluoroshield with DAPI (F6057; Merck). Images were collected in the tissue whole thickness with a confocal microscope (TCS SP5; Leica) with 1-μm *z*-axis steps by using ×20 dry and ×40 oil objectives. Maximum projections of adjacent fields were color-merged by using ImageJ software (38) and manually aligned in a continuous panorama using Adobe Photoshop Software.

Cross sections of lymphatic vessels at different sites were obtained by using the "reslice" function of the ImageJ software on the color-merged *z*-stacks.

Data analysis. Video recordings of spontaneous contractions of diaphragmatic lymphatics were converted to black and white binary images and were analyzed by using the "diameter" plugin (14) of the ImageJ software to obtain diameter over time profiles highlighting vessels' edges displacement during intrinsic contractility.

Quantification of f_{c-i} rate of change upon variations in tissue temperature was performed through calculation of the Q_{10} values that provide the reaction rate increase for every 10°C rise in temperature (18) as

$$Q_{10} = \left(\frac{f_{cT_2} - f_{cT_1}}{T_2 - T_1} \right)^{10} \quad (1)$$

where f_{cT2} and f_{cT1} were the contraction frequencies measured at temperature T_2 and T_1, respectively.

Diameter profiles were analyzed by Clampfit 10 Software (Molecular Devices) to evaluate the lymphatic intrinsic contraction frequency (f_c; cycles/min) over a period of ≥1 min and measure diastolic (d_d; μm) and systolic (d_s; μm) diameters for each contraction.

Contraction amplitude (Δd; μm) was computed as

$$\Delta d = d_d - d_s \quad (2)$$

and expressed as percentage of d_d.

Pleural diaphragmatic lymphatic vessels are ellipse shaped (25), and the transverse to parallel diameter ratio is 0.35 (21); thus, the changes in cross-sectional area (ΔS; μm^2) during intrinsic contractions could be computed as

$$\Delta S = \left\{\left[r_d \times \left(r_d \times 0.35\right) \times \pi\right]\right\} - \left\{\left[r_s \times \left(r_s \times 0.35\right)\right] \times \pi\right\} \quad (3)$$

being r_d (μm) and r_s (μm) diastolic and systolic radii, respectively.

The stroke volume (SV; pl) was computed in an ideal lymphatic tract of 105.50 μm (42) as

$$SV = \frac{\Delta S \times 105.50\mu m}{10^3} \quad (4)$$

being 10^3 the μm^3 to pl conversion factor. Then, intrinsic lymph flow (J_{lymph}, nL/min) was eventually easily estimated as

$$J_{lymph} = SV \times f_c \quad (5)$$

Statistical analysis. Data are presented as means ± SE. Statistics and data fitting were performed using SigmaPlot 10.0 Software (Systat Software) and Graphpad PRISM (version 5). Data significance was evaluated with unpaired Student's *t* test when two groups only were compared and one- or two-way ANOVA followed by Bonferroni's Multiple Comparison test where more groups were considered together (i.e., data in Figs. 3–5) after data normality distribution check. Statistical significance was set at $P < 0.05$.

RESULTS

In ex vivo diaphragmatic intrinsically contracting lymphatics ($n = 26$), the Q_{10} values of f_c varied between 0.4 and 30 in the temperature range 32–40°C (Fig. 1, black circles); data were fitted by the Gaussian peak equation

$$Q_{10} = 34.19 \times e^{\left[-0.5 \times \left(\frac{T - 36.47}{0.85}\right)^2\right]}$$

with $r^2 = 0.97$, centered at 36.47 ± 0.04°C, and with a Q_{10} peak of 34.19 ± 1.56.

For dermal vessels ($n = 5$), Q_{10} of f_c varied between 1 and 3 in the temperature range of 25–40°C and was fitted by the following Gaussian Peak equation

$$Q_{10} = 2.62 \times e^{\left[-0.5 \times \left(\frac{T - 31.03}{4.98}\right)^2\right]}$$

with $r^2 = 0.47$, centered at 31.03 ± 0.43°C, and with a Q_{10} peak of 2.62 ± 0.18 ($P < 0.01$ vs. diaphragmatic vessels, unpaired *t* test; $n = 31$).

TRPV1, -3, and -4 expression in diaphragmatic lymphatic vessels. Prox1 gene expression (Fig. 2*A*) was similar in both spontaneously contracting and not contacting vessel populations ($P = 0.2767$, unpaired *t* test; $n = 12$), confirming their lymphatic nature, whereas the relative expression of lymphatic muscle (LM) actin (Fig. 2*A*) was significantly higher (+1.8 times, $P < 0.05$, unpaired *t* test; $n = 12$) in the former. As shown in Fig. 2*B*, TRPV1 and TRPV3 gene expression was similar in contracting and not contracting vessels and was not significantly different from the transcript levels measured for both genes in DRGs. Instead, in both populations of diaphragmatic lymphatics, TRPV4 expression was similar ($P = 0.3609$, unpaired *t* test; $n = 12$) and significantly higher compared with DRGs ($P < 0.01$, +4.8- and +5.9-fold, respectively; $n = 12$).

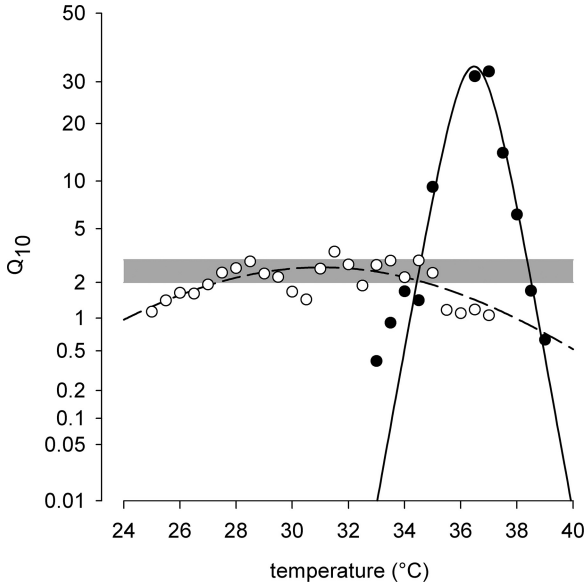

Fig. 1. Plot of the Q_{10} values of contraction frequency (f_c) variation in response to a +0.5°C change in temperature over the range of 33–40°C for diaphragmatic lymphatics (●; $n = 26$) and over the range of 25–40°C for dermal vessels (○; $n = 5$). Data were computed from the mean f_c values from experiments in Ref. 42 using *Eq. 1* (see MATERIALS AND METHODS). Gaussian fits of diaphragmatic vessel (solid line) and dermal vessel (dashed line) Q_{10} values were centered at 36.47°C and 31.03°C, respectively. Gray bar indicates the normal range of Q_{10} values for simple enzymatic reactions, according to Hille (16).

Effect of TRPV channel blocking on intrinsic lymphatic contractions. Control vessels (mean d_d 183.97 ± 31.81 μm, mean f_c at 35°C of 10.8 ± 1.0 cycles/min; $n = 10$) challenged with increasing temperature steps from 35 to 39°C showed the typical f_c sigmoidal increase (Fig. 3, gray circles) already documented (42). Intrinsic f_c data were fitted by the following sigmoidal curve (Fig. 3, solid line):

$$f_c = 10.15 \pm \frac{28.15 - 10.15}{1 + \left(\frac{36.99}{T}\right)^{54.65}}$$

with $r^2 = 0.99$; lower f_c asymptote: 10.15 ± 0.49 cycles/min; upper f_c asymptote: 28.15 ± 0.52 cycles/min; f_{c50} 36.99 ± 0.06°C (assuming f_{c50} as the equivalent of EC_{50}); Hill slope: 54.65 ± 5.26.

When challenged with 10 μM Ruthenium Red (RuR_{10}; Fig. 3), vessels exposed to increasing test temperatures started with an intrinsic f_c at 35°C not significantly different from control (hollow dots; mean d_d 140.95 ± 23.20 μm, mean f_c at 35°C of 11.0 ± 1.2 cycles/min; $n = 17$, 1-way ANOVA $P = 0.99$), which then was significantly lower than control f_c both at 37°C (10.4 ± 1.3 cycles/min for RuR_{10} vs. 19.3 ± 1.3 cycles/min in control, $P < 0.01$, 1-way ANOVA; $n = 17$) and at 39°C (10.4 ± 1.4 cycles/min for RuR_{10} vs. 27.0 ± 1.8 cycles/min in control, $P < 0.01$, 1-way ANOVA; $n = 17$).

Data from RuR_{10} experiments were fitted (Fig. 3, dashed line) by the linear regression

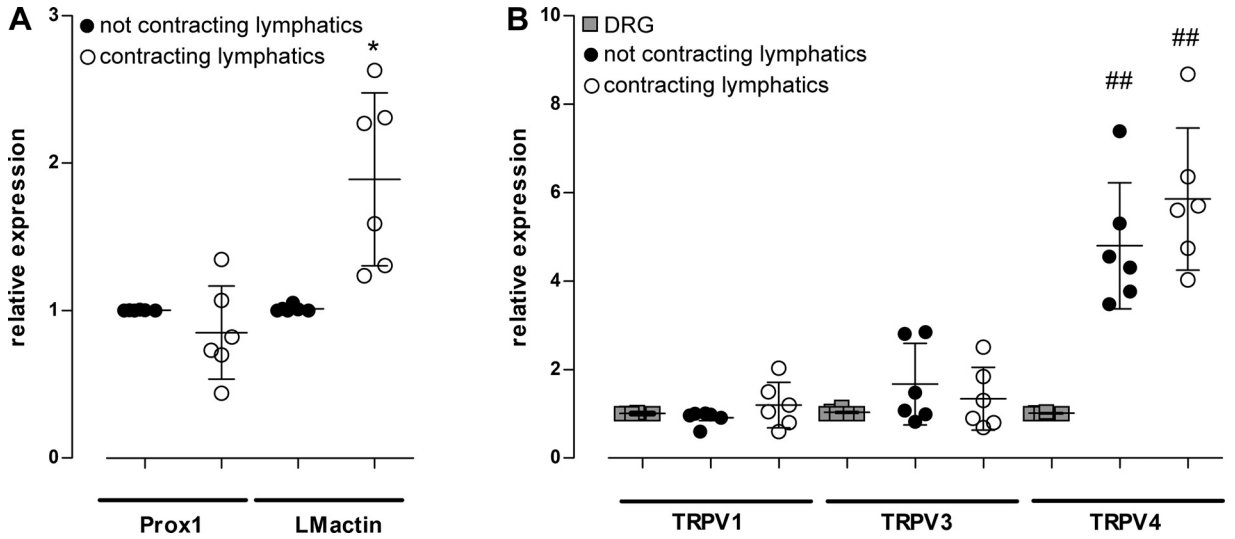

Fig. 2. *A*: relative expression of the lymphatic endothelial marker Prox1 and the lymphatic muscle (LM) actin in both contracting (○) and not contracting (●) lymphatics. Contracting vessels displayed significantly higher expression of LM with respect to not contracting ones evaluated by 2-way ANOVA, $P < 0.05$; $n = 6$. *B*: relative expression of transient receptor potential vanilloid (TRPV)1, TRPV3, and TRPV4 genes in contracting (○) and not contracting (●) lymphatics compared with the respective expression of TRPVs in dorsal root ganglions (DRGs; gray squares). TRPV4 channels were highly expressed in both contracting and not contracting vessels; $n = 6$ animals for all genes tested, 2-way ANOVA. *$P < 0.05$ vs. not contracting vessels; ##$P < 0.01$ vs. DRGs.

$$f_c = 12.83 - 0.05 \times T,$$

with $r^2 = 0.45$, f_c intercept at 12.83 ± 0.96 cycles/min, and slope factor of -0.05 ± 0.03 cycles/(min ·°C).

When challenged with 20 μM Ruthenium Red (RuR_{20}; Fig. 3, black circles), the intrinsic f_c of these diaphragmatic vessels (mean d_d 169.55 ± 34.78 μm, mean f_c at 35°C of 11.2 ± 1.2 cycles/min; $n = 6$, not significantly different from control vessels at 35°C, 1-way ANOVA, $P = 0.99$) decreased with increasing temperatures and was significantly lower than in control both at 37°C (8.8 ± 1.0 cycles/min for RuR_{20} vs. 19.3 ± 1.3 cycles/min in control, $P < 0.01$, 1-way ANOVA; $n = 16$) and at 39°C (7.3 ± 1.2 cycles/min for RuR_{20} vs. 27.0 ± 1.8 cycles/min in control, $P < 0.01$, 1-way ANOVA; $n = 16$). At 39°C, f_c in RuR_{20} was also lower, albeit not significantly, than the f_c value measured in RuR_{10} (7.3 ± 1.2 cycles/min for RuR_{20} vs. 10.4 ± 1.4 cycles/min for RuR_{10}, $P = 0.1273$, 1-way ANOVA among the 3 groups, $P = 0.27$; $n = 13$). Data from RuR_{20} experiments were fitted (Fig. 3, dotted line) by the following dose-response curve:

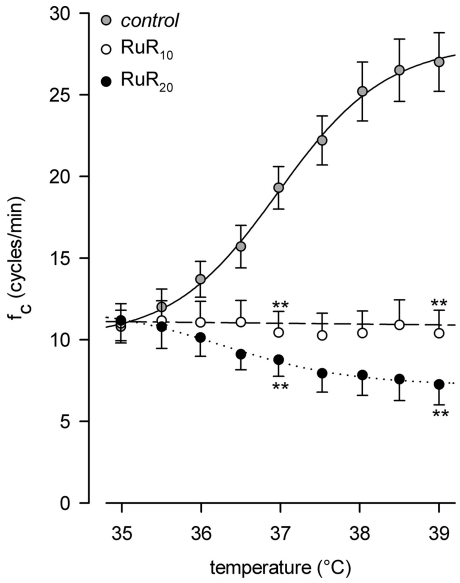

Fig. 3. Effect of the nonselective transient receptor potential vanilloid (TRPV) channel antagonist Ruthenium Red (RuR) on lymphatic intrinsic contraction frequency (f_c). Control vessels ($n = 10$; gray circles and solid line) displayed an increase in f_c with increasing temperatures from 35 to 39°C. RuR_{10} ($n = 7$; ○ and dashed line) perfusion resulted in an almost constant f_c for all of the temperatures tested, whereas RuR_{20} ($n = 6$, ● and dotted line) reduced f_c. **$P < 0.01$ with respect to control at the same temperature, 1-way ANOVA; $n = 17$ for RuR_{10} and 16 for RuR_{20}.

$$f_c = 7.20 \pm \frac{11.16 - 7.20}{1 + \left(\frac{36.31}{T}\right)^{-46.01}}$$

with $r^2 = 0.99$; upper f_c asymptote: 11.16 ± 0.23 cycles/min; lower f_c asymptote: 7.20 ± 0.23 cycles/min; IC_{50}: 36.31 ± 0.20°C; Hill slope: −46.01 ± 10.85.

Mean d_d did not vary significantly ($P = 0.607$, 1-way ANOVA) among control, RuR_{10}, and RuR_{20} contracting vessel groups.

Because even the lower RuR dose (RuR_{10}) was able to exert a statistically significant effect, to avoid any not specific effect due to overdosage of the drug, further comparisons between control, RuR, and HC groups were performed considering RuR 10 μM data.

Effect of TRPV4-selective block on intrinsic lymphatic contractions. The effect of 2.5 μM HC-067047 (group $HC_{2.5}$), a selective TRPV4 channel antagonist, on the intrinsic f_c of contracting diaphragmatic lymphatics (mean d_d 138.57 ± 15.54 μm, mean f_c at 35°C of 10.0 ± 0.6 cycles/min; $n = 4$) was described (Fig. 4; open squares) by the linear fit (Fig. 4, dashed line)

$$f_c = 11.06 - 0.03 \times T$$

with $r^2 = 0.04$, the f_c intercept at 11.06 ± 1.86 cycles/min, and a slope factor of −0.03 ± 0.05 cycles/(min·°C). $HC_{2.5}$ signif-

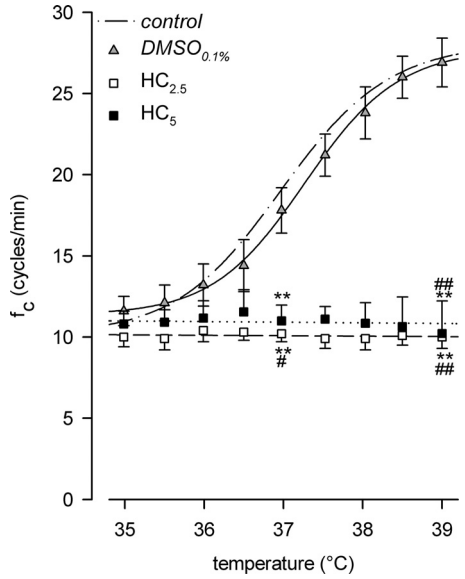

Fig. 4. Effect of the selective transient receptor potential channels of the vanilloid 4 subfamily (TRPV4) channel blocker HC-067047 (HC) on lymphatic intrinsic contraction frequency (f_c). Vehicle-only perfused lymphatics ($DMSO_{0.1\%}$; $n = 5$; gray triangles and solid line) displayed an increase in f_c with increasing temperatures, from 35 to 39°C, superimposable to that obtained in control vessels ($n = 10$; dashed/dotted line, plot from Fig. 3). Addition of both $HC_{2.5}$ ($n = 4$, □ and dashed line) and HC_5 ($n = 3$; ■ and dotted line) resulted in the attainment of a constant f_c for every temperature tested. $^{**}P < 0.01$, 1-way ANOVA with respect to control; $^{\#}P < 0.05$, 1-way ANOVA with respect to $DMSO_{0.1\%}$; $^{\#\#}P < 0.01$, 1-way ANOVA with respect to $DMSO_{0.1\%}$.

icantly decreased intrinsic f_c versus control both at 37°C (10.2 ± 0.5 cycles/min for $HC_{2.5}$ vs. 19.3 ± 1.3 cycles/min in control, $P < 0.01$, 1-way ANOVA; $n = 14$) and at 39°C (10.0 ± 0.7 cycles/min for $HC_{2.5}$ vs. 27.0 ± 1.8 cycles/min in control, $P < 0.01$, 1-way ANOVA; $n = 14$). When vessels were challenged with 5 μM HC-067047 (group HC_5; Fig. 4, black squares; mean d_d 127.95 ± 14.90 μm, mean f_c at 35°C of 10.8 ± 0.8 cycles/min; $n = 3$), the intrinsic f_c remained almost constant at the value displayed at 35°C according to the linear fit (Fig. 4, dotted line)

$$f_c = 12.32 - 0.04 \times T$$

with $r^2 = 0.08$, the f_c intercept at 12.32 ± 2.11 cycles/min, and a slope factor of -0.04 ± 0.06 cycles/(min °C).

HC_5 significantly reduced intrinsic f_c with respect to control both at 37°C (11.0 ± 1.0 cycles/min for HC_5 vs. 19.3 ± 1.3 cycles/min in control, $P < 0.01$, 1-way ANOVA; $n = 13$) and at 39°C (10.2 ± 2.0 cycles/min for HC_5 vs. 27.0 ± 1.8 cycles/min in control, $P < 0.01$, 1-way ANOVA; $n = 13$). Because no significant f_c differences were found between $HC_{2.5}$ and HC_5 at any tested temperature (2-way ANOVA among f_c of $HC_{2.5}$ and HC_5 groups at every tested temperature), in the successive experiments the lowest dose was used for comparison with both control and RuR_{10} groups.

Data obtained by applying the same temperature step increase protocol to vessels bathed by vehicle alone ($DMSO_{0.1\%}$ group, mean d_d 142.22 ± 10.36 μm; $n = 5$) were fitted (Fig. 4, gray triangles and solid line) by the dose-response curve

$$f_c = 11.37 \pm \frac{27.78 - 11.37}{1 + \left(\frac{37.28}{T}\right)^{63.57}}$$

with $r^2 = 0.99$; lower f_c asymptote: 11.37 ± 0.24 cycles/min; upper f_c asymptote: 27.78 ± 0.28 cycles/min; EC_{50}: 37.28 ± 0.04°C; Hill slope:63.57 ± 4.37. No significant differences in intrinsic f_c were found between $DMSO_{0.1\%}$ and control (Fig. 4, dashed/dotted line, 2-way ANOVA among the 2 groups for every temperature tested), whereas f_c measured in presence of $HC_{2.5}$ and HC_5 was significantly lower than the values recorded in $DMSO_{0.1\%}$ both at 37°C (10.2 ± 0.5 cycles/min for $HC_{2.5}$, 11.0 ± 1.0 cycles/min for HC_5 vs. 17.8 ± 1.4 cycles/min for $DMSO_{0.1\%}$; $P < 0.05$, 1-way ANOVA; $n = 9$ for $HC_{2.5}$ and $P < 0.01$ 1-way ANOVA; $n = 8$ for HC_5) and at 39°C (10.0 ± 0.7 cycles/min for $HC_{2.5}$, 10.2 ± 2.0 cycles/min for HC_5 vs. 26.9 ± 1.5 cycles/min for $DMSO_{0.1\%}$, $P < 0.01$ 1-way ANOVA; $n = 9$ for $HC_{2.5}$ and $n = 8$ for HC_5).

Mean d_d did not vary significantly ($P = 0.536$, 1-way ANOVA) among the $HC_{2.5}$, HC_5, and $DMSO_{0.1\%}$ groups.

Effect of TRPV channel blockage on contraction amplitude. The increase in intrinsic f_c recorded after increasing temperature steps from 35 to 39°C were applied in control conditions ($n = 10$) was associated with a decrease in lymphatic vessel amplitude (Δd) from $31.1 \pm 3.2\%$ of d_d at 35°C to $17.9 \pm 3.2\%$ of d_d at 39°C. Control Δd data (Fig. 5*A*, gray circles) were fitted (Fig. 5*A*, solid line) by the dose-response curve

$$\Delta d = 17.89 \pm \frac{31.00 - 17.89}{1 + \left(\frac{37.09}{T}\right)^{-79.48}}$$

with $r^2 = 0.99$; upper asymptote: $31.00 \pm 0.27\%$ of d_d; lower asymptote: $17.89 \pm 0.31\%$ of d_d; IC_{50}: 37.09 ± 0.05°C (assuming the temperature as an antagonist for Δd); Hill slope: -79.48 ± 7.50).

When the same temperature protocol was applied to the RuR_{10} group ($n = 7$), Δd decreased again (Fig. 5*A*; open circles) with increasing temperatures from $29.9 \pm 4.8\%$ of d_d at 35°C to $25.1 \pm 3.5\%$ of d_d at 39°C. However, Δd decrease was lower, albeit not statistically significant, in the RuR_{10} group than in control group both at 37°C ($27.4 \pm 4.0\%$ of d_d for RuR_{10} vs. $25.0 \pm 3.3\%$ of d_d for control, $P = 0.6493$ 1-way ANOVA; $n = 17$) and at 39°C ($25.1 \pm 3.5\%$ of d_d for RuR_{10} vs. $17.9 \pm 3.2\%$ of d_d for control, $P = 0.1561$ 1-way ANOVA; $n = 17$). RuR_{10} Δd data were fitted (Fig. 5*A*, dotted line) by the dose-response curve

$$\Delta d = 24.99 \pm \frac{30.05 - 24.99}{1 + \left(\frac{36.95}{T}\right)^{-116.75}}$$

with $r^2 = 0.98$; upper asymptote: $30.05 \pm 0.25\%$ of d_d; lower asymptote: $24.99 \pm 0.25\%$ of d_d (significantly higher than control, $P < 0.01$, unpaired t test; $n = 17$); IC_{50}: 36.95 ± 0.09°C; Hill slope: -116.75 ± 30.81.

The $HC_{2.5}$ group displayed a reduction in Δd from $30.1 \pm 2.9\%$ of d_d at 35°C to $23.4 \pm 2.0\%$ of d_d at 39°C, albeit one less pronounced than in control group, both

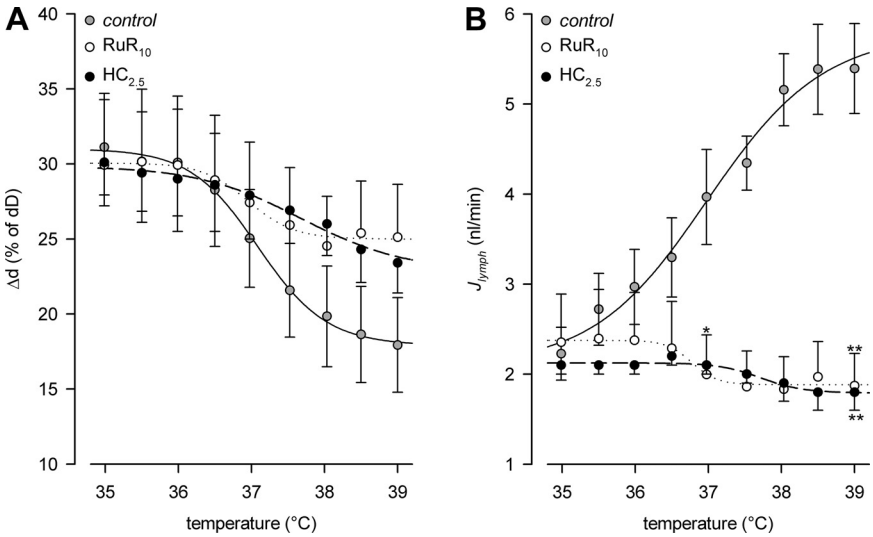

Fig. 5. *A*: effect of the nonselective transient receptor potential vanilloid (TRPV) channel antagonist Ruthenium Red $(RuR)_{10}$ ($n = 7$; ○ and dotted line) and the selective TRPV4 channel blocker $HC_{2.5}$ ($n = 4$; ● and dashed line) on lymphatic Δd, expressed as $\%d_d$. Control vessels ($n = 10$; gray circles and solid line) displayed a decrease in Δd with increasing temperatures from 35 to 39°C. Both RuR_{10} and $HC_{2.5}$ perfusions attenuated the Δd decrease. *B*: effect of RuR_{10} ($n = 7$; ○ and dotted line) and $HC_{2.5}$ ($n = 4$; ● and dashed line) on lymphatic intrinsic J_{lymph}. Control vessels ($n = 10$; gray circles and solid line) displayed a J_{lymph} increase with increasing temperatures from 35 to 39°C. Both RuR_{10} and $HC_{2.5}$ perfusions resulted in a nonsignificant decrease in J_{lymph} with respect to the values obtained at 35°C. $^*P < 0.05$, 1-way ANOVA with respect to control; $^{**}P < 0.01$, 1-way ANOVA with respect to control.

measured at 37°C (27.9 ± 2.9% of d_d for $HC_{2.5}$ vs. 25.0 ± 3.3% of d_d for control, $P = 0.6149$, 1-way ANOVA; $n = 14$) and at 39°C (23.4 ± 2.0% of d_d for $HC_{2.5}$ vs. 17.9 ± 3.2% of d_d for control, $P = 0.3214$, 1-way ANOVA; $n = 14$). $HC_{2.5}$ Δd data (Fig. 5*A*, black circles) were fitted (Fig. 5*A*, dashed line) by the following dose-response curve

$$\Delta d = 22.79 \pm \frac{29.84 - 22.79}{1 + \left(\frac{37.70}{T}\right)^{-52.37}}$$

with $r^2 = 0.99$; upper asymptote: 29.84 ± 0.21% of d_d; lower asymptote: 22.79 ± 0.49% of d_d, IC_{50} 37.70 ± 0.15°C; Hill slope: −52.37 ± 9.03. The lower asymptote was significantly higher than control ($P < 0.01$, 1-way ANOVA; $n = 14$) but significantly lower than RuR_{10} ($P < 0.01$, 1-way ANOVA; $n = 11$); IC_{50} was significantly higher than control IC_{50} ($P < 0.01$, unpaired *t* test; $n = 14$); the Hill slope was not statistically different from either to RuR_{10} or control group ($P = 0.161$ and $P = 0.063$, 1-way ANOVA; $n = 11$ and $n = 14$, respectively).

Effect of TRPV channel block on lymph flow. Lymph flow (J_{lymph}) was computed for the control, RuR_{10}, and $HC_{2.5}$ groups by means of *Eq. 5*. In the control group (Fig. 5*B*, gray circles; $n = 10$), J_{lymph} increased with increasing temperature from 2.2 ± 0.3 nL/min at 35°C to 5.4 ± 0.9 nL/min at 39°C. J_{lymph} data were fitted (Fig. 5*B*, solid line) by the dose-response curve

$$J_{lymph} = 2.11 \pm \frac{5.80 - 2.11}{1 + \left(\frac{37.01}{T}\right)^{46.93}}$$

with $r^2 = 0.99$; lower J_{lymph} asymptote: 2.11 ± 0.33 nL/min; upper J_{lymph} asymptote: 5.80 ± 0.36 nL/min; EC_{50}: 37.01 ± 0.18°C; Hill slope: 46.93 ± 13.76.

On the contrary, in the RuR_{10} group (Fig. 5*B*, open circles; $n = 7$), J_{lymph} significantly decreased with increasing temperatures, from 2.4 ± 0.5 nL/min at 35°C to 1.9 ± 0.4 nL/min at 39°C ($P < 0.01$ vs. control, 1-way ANOVA; $n = 17$). J_{lymph} data for RuR_{10} were fitted (Fig. 5*B*, dotted line) by the dose-response curve

$$J_{lymph} = 1.88 \pm \frac{2.38 - 1.88}{1 + \left(\frac{36.78}{T}\right)^{-211.00}}$$

with $r^2 = 0.97$; upper J_{lymph} asymptote: 2.38 ± 0.03 nL/min; lower J_{lymph} asymptote: 1.88 ± 0.03 nL/min (significantly lower than control at the higher temperature, $P < 0.01$, unpaired *t* test; $n = 17$); IC_{50}: 36.78 ± 0.09°C; Hill slope: −211.00 ± 72.86.

In the $HC_{2.5}$ group (Fig. 5*B*, black circles; $n = 4$) J_{lymph} values remained almost constant at all tested temperatures, ranging from 2.1 ± 0.1 nL/min at 35°C to 1.8 ± 0.2 nL/min at 39°C (significantly lower than control, $P < 0.05$, unpaired *t* test; $n = 14$). J_{lymph} data for $HC_{2.5}$ were fitted (Fig. 5*B*, dashed line) by the dose-response curve

$$J_{lymph} = 1.79 \pm \frac{2.12 - 1.79}{1 + \left(\frac{37.72}{T}\right)^{-130.48}}$$

with $r^2 = 0.95$; higher J_{lymph} value: 2.12 ± 0.02 nL/min; lower J_{lymph} value: 1.79 ± 0.04 nL/min; IC_{50}: 37.72 ± 0.17°C; Hill slope: −130.48 ± 63.98.

Lower J_{lymph} value was similar to RuR_{10} but significantly lower than control at the higher temperature ($P < 0.01$, 1-way ANOVA; $n = 14$), and the IC_{50} was significantly higher than control ($P < 0.05$, 1-way ANOVA; $n = 14$).

Effect of TRPV4 channel activation on lymphatic intrinsic contractility. To confirm the observed almost exclusive involvement of TRPV4, we assessed the modification of f_c, Δd, and J_{lymph} due to TRPV4 activation by means of its selective agonist GSK1016790A at a constant temperature of 35°C. In the GSK101 group, the mean d_d (148.58 ± 21.05 μm; $n = 6$) did not significantly differ from the value of control vessels (183.97 ± 31.81 μm, $P = 0.4406$, unpaired *t* test; $n = 16$). Increasing concentrations of GSK1016790A (from 50 nM to 350 nM) at 35°C (Fig. 6*A*, black diamonds) induced a concen-

tration-dependent enhancement of f_c from the basal level of 10.2 ± 0.8 cycles/min in the absence of the drug (Fig. 6*A*, gray diamonds) to 26.7 ± 1.2 cycles/min with 350 nM GSK101. This latter value was superimposable to that observed at 39°C in control conditions (27.0 ± 1.8 cycles/min, $P = 0.9071$, unpaired t test; $n = 16$) and was significantly higher than f_c recorded in the presence of the vehicle-only ($DMSO_{0.01\%}$ group; $n = 4$) at 35°C ($f_c = 11.0 \pm 2.1$ cycles/min in $DMSO_{0.01\%}$; $P < 0.01$, GSK101 vs. $DMSO_{0.01\%}$ unpaired t test; $n = 10$). Data for f_c increase due to GSK101 were fitted (Fig. 6*A*, solid line) by the dose-response curve

$$f_c = 10.44 \pm \frac{29.00 - 10.44}{1 + \left(\frac{142.30}{\text{GSK101}}\right)^{2.09}}$$

with $r^2 = 0.99$; lower f_c asymptote: 10.44 ± 0.61 cycles/min; upper f_c asymptote: 29.00 ± 1.86 cycles/min; EC_{50}: 142.30 ± 16.86 nM GSK101; Hill slope: 2.09 ± 0.41). Both lower ($P = 0.7191$, unpaired t test; $n = 16$) and upper ($P = 0.5949$, unpaired t test; $n = 16$) asymptotes were not significantly different from those obtained for the dose-response curve of control vessels subjected to temperature increments from 35 to 39°C.

As GSK101 increased intrinsic f_c to an extent similar to control, the contractile cycle period decreased similarly in both experimental groups, critically shortening the diastolic filling phase. We then analyzed whether any difference could be found in the systolic time, pointing out that increasing temperature (1.10 ± 1.00 s at 35°C and 0.78 ± 0.08 s at 39°C; $n = 10$ vessels), but not GSK101 perfusion at a constant 35°C (1.01 ± 0.09 s at GSK101: 0 nM; 1.02 ± 0.09 at GSK101: 350 nM; $n = 6$ vessels), altered this parameter.

GSK101 induced also a concentration-dependent reduction of Δd (Fig. 6*B*, black diamonds) from 33.0 ± 2.8% of d_d in the absence of the drug (Fig. 6*B*, gray diamonds) to 18.9 ± 2.8% of d_d at 350 nM GSK101. This latter value was similar to the Δd lower plateau displayed by control vessels exposed to 39°C (17.9 ± 3.2% of d_d, $P = 0.8344$, unpaired t test; $n = 16$). GSK101 Δd data were fitted (Fig. 6*B*, solid line) by the dose-response curve

$$\Delta d = 17.09 \pm \frac{32.44 - 17.09}{1 + \left(\frac{139.40}{\text{GSK101}}\right)^{-2.53}}$$

with $r^2 = 0.97$, upper asymptote: 32.44 ± 1.51% of d_d; lower asymptote: 17.09 ± 3.61% of d_d; IC_{50}: 139.40 ± 34.60 nM GSK101; Hill slope −2.53 ± 1.43.

Again, also in the case of Δd, lower ($P = 0.7761$, unpaired t test; $n = 16$) and upper ($P = 0.2481$, unpaired t test; $n = 16$) asymptotes were not significantly different from those obtained when fitting Δd of control vessels exposed to increasing temperatures up to 39°C.

Because intrinsic f_c increased and Δd decreased, both in a dose-dependent manner in response to GSK101 application, increasing concentrations of GSK101 also affected J_{lymph} (Fig. 6*C*, black diamonds). Starting from a mean J_{lymph} value of 2.3 ± 0.4 nL/min in the absence of the drug (Fig. 6*C*, gray diamonds), it progressively increased up to 5.3 ± 0.9 nL/min at 350 nM GSK101 (the same upper J_{lymph} previously obtained in control vessels at 39°C, $P = 0.9425$, unpaired t test; $n = 16$). J_{lymph} data for GSK101 experiments were fitted (Fig. 6*C*, solid line) by the dose-response curve

$$J_{lymph} = 2.35 \pm \frac{5.72 - 2.35}{1 + \left(\frac{131.04}{\text{GSK101}}\right)^{2.18}}$$

with $r^2 = 0.99$; lower J_{lymph} asymptote: 2.35 ± 0.19 nL/min; upper J_{lymph} asymptote: 5.72 ± 0.48 nL/min; EC_{50}: 131.04 ± 22.27 nM GSK101; Hill slope: 2.18 ± 0.68). Both lower ($P = 0.6064$, unpaired t test; $n = 16$) and upper ($P = 0.8949$,

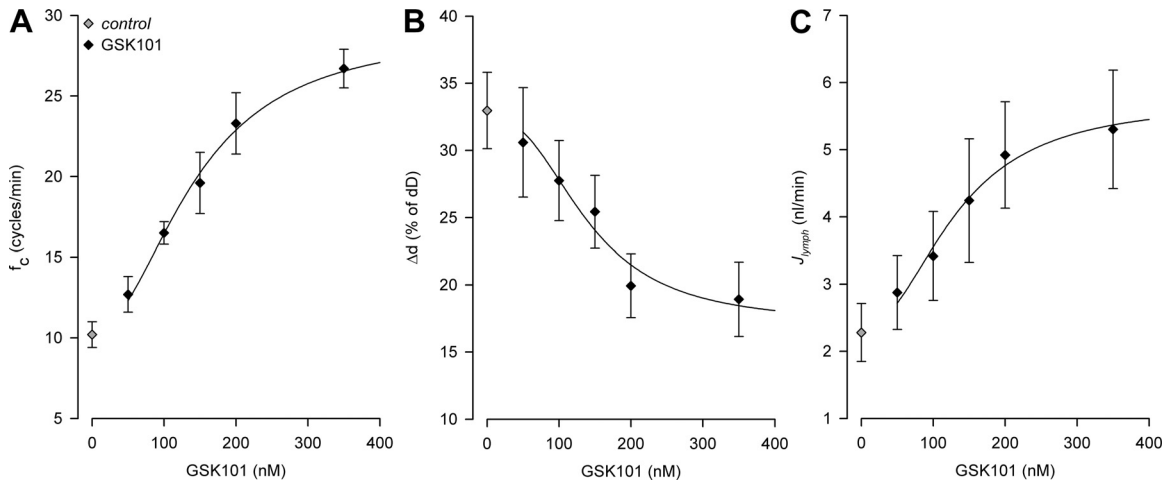

Fig. 6. *A*: effect of increasing concentrations of the selective transient receptor potential channels of the vanilloid 4 subfamily (TRPV4) agonist GSK101(50–350 nM, $n = 6$; ◆) on lymphatic intrinsic contraction frequency (f_c). Vessels, maintained at a constant temperature of 35°C and challenged with increasing concentrations of GSK101, displayed an increase in f_c similar to control vessels exposed to increasing temperatures. Gray diamond, intrinsic f_c recorded at 35°C in the absence of the drug. *B*: effect of GSK101 on intrinsic Δd. Increasing concentrations of GSK101 ($n = 6$, ◆) induced a decrease in Δd similar to what has been obtained when control vessels were exposed to increasing temperatures. Gray diamond, Δd measured at 35°C in the absence of the drug. *C*: GSK101 overall effect on intrinsic J_{lymph}. Lymphatic vessels exposed to increasing concentrations of GSK101 ($n = 6$; ◆) displayed an increase in J_{lymph}, reaching an upper plateau superimposable to the one of control vessels challenged with increasing temperatures. Gray diamond, J_{lymph} mean value, computed at 35°C in the absence of the drug.

unpaired t test; $n = 16$) asymptotes were not significantly different from those obtained in control conditions.

Localization of TRPV4 channels in the lymphatic vessel wall. To localize TRPV4 channel in the lymphatic vessel wall (i.e., either on lymphatic muscle and/or on endothelial cells), the distribution of TRPV4 channels along the lymphatic vessel wall was investigated by immunofluorescent staining on whole mount diaphragmatic specimens containing lymphatic vessels previously in vivo (FITC-filled; see MATERIALS AND METHODS for details). Figure 7 shows a reconstruction of a lymphatic segment obtained by aligning confocal images of several adjacent fields, where the red signal and white dots highlight the LM surrounding the vessel and TRPV4 channels, respectively, whereas the green signal is due to the residual FITC-dextran molecules adherent to the intraluminal-facing endothelial cells. As shown in Fig. 7, *boxes a′* and *b′*, at higher magnification (corresponding to Fig. 7, *sites a* and *b* of the main panel, respectively), white signal seems to strongly colocalize with FITC-dextran, as pointed out by arrowheads. Cross sections obtained at different positions (*c′–f′*, corresponding to *sites c–f*, respectively) highlight the LM organization surrounding the vessel lumen and support the hypothesis that TRPV4 channels are preferentially, if not exclusively, located on the lymphatic endothelium rather than on LM.

DISCUSSION

Q_{10} and the quest for the molecular sensor for temperature. The present temperature dependence of f_c in spontaneously contracting lymphatic vessel confirms our previous observation (42) attained in both diaphragmatic and dermal lymphatics, although the former vessels displayed a steeper ($0.62°C \cdot cycles^{-1} \cdot min^{-1}$) f_c versus temperature sigmoidal relationship compared with dermal ones [2.32°C/(cycles/min)]. Based on the general notion of the temperature dependence of biochemical reactions and considering the intrinsic f_c as the final "product" of a complex set of biochemical and mechanical pathways, we thought that calculation of the Q_{10} value of f_c in different populations of spontaneously contracting lymphatics might provide some hints on the mechanisms involved in f_c modulation. Hence, in addition to the Q_{10} value obtained in the present study for diaphragmatic lymphatics (Fig. 1, black circles and solid line), we used *Eq. 1* to calculate the Q_{10} value in dermal lymphatics, using data from our previously published paper (Fig. 1, open circles and dashed line). In dermal lymphatics, Q_{10} of f_c ($n = 5$) was much lower compared with diaphragmatic ones, varying between 1 and 3 in the temperature range of 25–40°C.

Because Q_{10} values exceeding 2–3 likely involve active mechanisms such as ionic channels (18), we next investigated the expression of TRPV1, TRPV3, and TRPV4 channels (11) in diaphragmatic lymphatics. Indeed, although both lymphatic vessels populations displayed a temperature-dependent variation of f_c, the much higher Q_{10} values (Fig. 1, black circles) revealed that a possible role for active mechanisms was more likely to occur in the diaphragmatic than in dermal vessels, whose lower Q_{10} values are typical for the gating mechanism of most ion channels (16).

TRPV channels are likely to be involved in temperature-dependent phenomena. Indeed, some of their isoforms (V1, but especially V3 and V4) have proven to be sensitive to temperature changes in other tissues (12) and are active in the range of temperatures experienced by tissues belonging to the ther-

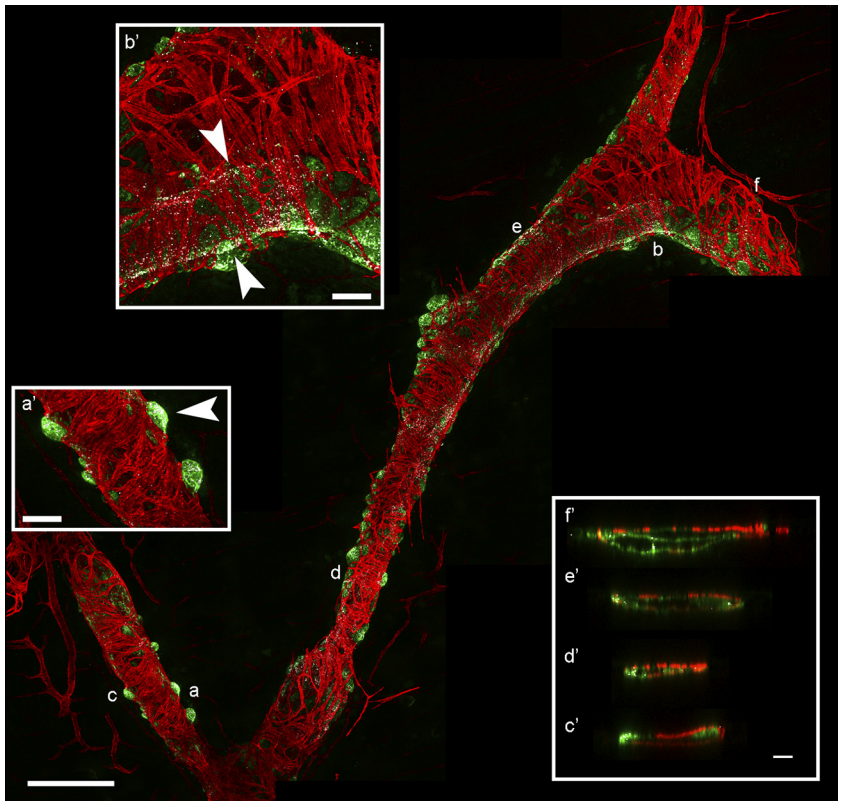

Fig. 7. Whole mount immunofluorescence assay to evaluate lymphatic muscle (LM; red signal) and transient receptor potential channels of the vanilloid 4 subfamily (TRPV4) channel (white signal) distribution on lymphatic vessels displaying residual FITC-dextran (green signal) lining vessel endothelium. *Insets a′* and *b′* (corresponding to *sites a* and *b*) and *cross-sections c′–f′* (corresponding to *sites c–f*) suggest a strong colocalization between TRPV4 channels and lymphatic endothelium, as pointed out by arrowheads. Scale bar, 250 μm. *Inset a′* and *b′* scale bars, 50 μm; *inset c′–f′* scale bars, 25 μm.

mal core, including diaphragmatic lymphatics (11). Hence, we assessed the level of expression of TRPV1, TRPV3, and TRPV4 mRNAs in the population of contracting and not contracting diaphragmatic lymphatic vessels; TRPV2 channels were not investigated since, because of their high-threshold temperature of activation (>52°C), they are more likely involved in noxious heat sensation (10). qRT-PCR analysis revealed that TRPV4 channel expression was five- to sixfold higher in diaphragmatic lymphatics (Fig. 2*B*) than in control DRG neurons (9, 54), whereas TRPV3 and TRPV1 channel expression was much lower, and their transcript levels were more similar to those observed in DRG neurons. In addition, TRPV1 channels have a temperature threshold of ~41°C, which made them less likely to be active in the 35–39°C physiological temperature range.

TRPV channel blockade. The temperature dependence seemed reduced or even abolished when lymphatic vessels were treated with TRPV antagonists. Indeed, at each dose used, the unselective TRPV channel antagonist Ruthenium Red (RuR; see Ref. 32a) completely abolished the f_c increase (Fig. 3) with increasing temperatures. To avoid TRPVs sensitization or desensitization-related artifacts (52), the different temperatures have always been applied in an increasing order in all of the experiments.

The decrease in contraction frequency observed during RuR_{20} perfusion might be due to an additional block (due to the higher dose used) on TRPV1 and/or TRPV3, which are indeed expressed in diaphragmatic lymphatics at levels comparable with the ones of DRGs (see Fig. 2).

However, if anything, the eventual block on TRPV3 could be the most probable cause of the reduction of contraction frequency given that the effect starts at ~36°C, a temperature closer to TRPV3 range of activity rather than TRPV1 one.

Similarly, when TRPV4 channels were selectively blocked by perfusing contracting lymphatics with HC-067047 (HC), a highly selective TRPV4 antagonist (13), f_c became temperature independent (Fig. 4), unlike what was found in control conditions and in the presence of vehicle-alone ($DMSO_{0.1\%}$). Because the selective block of TRPV4 caused a complete abolishment of f_c temperature dependence, it is likely that this specific channel isoform is the most direct and efficient among the TRPV channel family in determining the response of intrinsic lymphatic f_c to temperature.

As already reported (42), in control conditions, when temperature was raised up to 39°C, the f_c increase was accompanied with a decrease in contraction amplitude (Δd), which in turn caused a reduction in lymphatic stroke volume (SV). This response seemed to be a critical temperature-related mechanism; indeed, when lymphatics were held at a constant temperature, changes in fluid osmolarity deeply affected intrinsic f_c but not Δd and SV (43). At variance with the significant flattening of f_c values obtained in the presence of both drugs (as the data in Figs. 3 and 4 show), the negative relationship between f_c and Δd was attenuated (Fig. 5*A*) but not completely abolished when tissue specimens were perfused with either RuR_{10} or $HC_{2.5}$. This discrepancy might point to the fact that the role of TRPV4 channels is predominantly linked to the pacemaker mechanism rather than to the contraction mechanism itself. The uncovering of the signaling mechanism underlying this effect stands beyond the scope of the present work and would deserve a more detailed investigation at the cellular level, which, however, cannot be carried out in our ex vivo experimental setup. However, given that lymph flow (J_{lymph}) is strictly related to both f_c and contraction amplitude (*Eqs. 2–5*), blockade of TRPV4, either selective or not, led to a marked decrease of J_{lymph} compared with values observed in control conditions (Fig. 5*B*). The net effect of the selective blockade by HC is similar to that observed with the unselective antagonist RuR, a further clue of the predominant role of TRPV4 among TRPV channels in the response to temperature.

TRPV4 channel activation at constant temperature. To better confirm the role of TRPV4 channels in shaping the response of f_c to temperature, we replicated the temperature-dependent increase in f_c in the presence of increasing concentrations of its potent and selective agonist GSK1016790A (45) at the constant temperature of 35°C to avoid possible artifacts due to the interplay of different stimuli (i.e., either physiological, such as temperature, or pharmacological, such as GSK101) acting on the very same TRPV4 channels. Indeed, the response of f_c to increasing concentrations of GSK101 closely resembled the normal response to increasing steps of temperature in control lymphatics (Fig. 6*A*). Interestingly, the contraction amplitude (Fig. 6*B*) varied in a fashion that closely matched the control traces of Fig. 5*A*. Moreover, as additional evidence to confirm the hypothesis that TRPV4 channels are predominantly linked to the pacemaker mechanism, a closer analysis of how the intrinsic f_c was increased by both temperature and GSK101 showed that, whereas diastolic time decreased in both cases, the systolic period was modified only by temperature. Nevertheless, increasing GSK101 concentrations deeply affected J_{lymph} (Fig. 6*C*), which varied in a manner closely matching the control response trace. Interestingly, it was possible to plot on the same graph J_{lymph} values obtained in the presence of increasing GSK101 concentrations at 35°C (Fig. 8, black diamonds) and those obtained by increasing temperature in

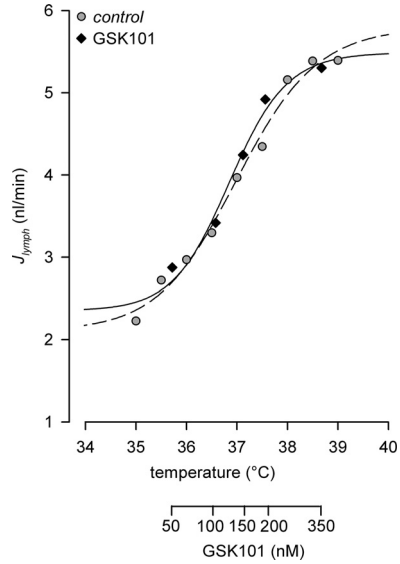

Fig. 8. Comparison of J_{lymph} increase obtained in response to increasing temperatures in control conditions (n = 10; gray circles) and in response to increasing concentrations of GSK101 in lymphatics held at the constant temperature of 35°C (n = 6; ◆), showing almost an equivalence in the 2 plots. GSK101 dose to temperature matching was obtained by contraction frequency (f_c) vs. temperature and f_c vs. GSK101 nM curves in Figs. 3 and 6*A*, respectively.

control vessels (Fig. 8, gray cicrcles) substantially obtaining two superimposable curves. Is it worth noting that under no circumstances did noncontracting vessels exposed to increasing temperatures or GSK101 begin to display intrinsic contractions, thus indirectly confirming our previous findings that these lymphatic vessels do not possess an adequate contracting machinery (31).

Localization of TRPV4 channels on the lymphatic vessel walls. Functional assays were not informative about the localization of TRPV4 channels along the wall of lymphatic vessels. Because TRPV4 channel mRNA levels were similar in contracting and not contracting vessels (Fig. 2*B*), mRNA expression data suggested a possible endothelial localization of the channel (Fig. 2*A*), as also verified with immunostaining (Fig. 7). Indeed, the TRPV4 signal was more colocalized with the FITC signal defining the inner limits of the lymphatic vessels (lining the endothelial cells) and to a negligible degree with the LM actin staining, which shows their disposition on the outer lymphatic musculature, as previously reported also in popliteal collecting lymphatics (2). These data might imply that endothelial cells might be the source of the TRPV4-derived temperature signal, which is then conveyed to lymphatic muscle cells to exert its effect.

Conclusions. The present data show that TRPV4 channels are predominantly expressed by diaphragmatic lymphatic vessels, and their selective block leads to the complete absence of the temperature-dependent modulation of f_c and J_{lymph} normally displayed by intrinsically contracting lymphatics. TRPV4-selective activation mimics the normal behavior of lymphatics subjected to temperature changes in the physiological range from 35 to 39°C for the thermal core, even in stressful conditions, such as it occurs during intense exercise in extreme conditions or fasting, opening a possible translational implication of a pharmacological access to increase lymphatic intrinsic pumping. Indeed, the possibility to modify f_c, and thus J_{lymph}, by means of selective TRPV4 channel agonist/antagonists may represent a useful pharmacological approach aiming to ameliorate pathological conditions associated with mild interstitial edema by increasing the efficiency of the lymphatic intrinsic pump without affecting the liquid filtration process at the blood capillaries' endothelial layer. Moreover, whole mount immunostaining showed a predominant localization of TRPV4 channels on the lymphatic endothelial cells, suggesting future research on the signaling mechanism that could link the endothelial-derived message arising from TRPV4 channels to the lymphatic musculature to modulate contraction frequency.

GRANTS

We thank Prof. Elena Bossi and Dr. Cristina Roseti, Laboratory of Cellular and Molecular Physiology, Department of Biotechnology and Life Sciences, University of Insubria, Varese, for kindly providing GSK1016790A used in the present work.

DISCLOSURES

No conflicts of interest, financial or otherwise, are declared by the authors.

AUTHOR CONTRIBUTIONS

A.M. conceived and designed research; E.S., C.M., M.B., A.B., and C.G. performed experiments; E.S. analyzed data; E.S., C.G., and A.M. interpreted results of experiments; E.S., M.B., and A.B. prepared figures; E.S. and A.M. drafted manuscript; E.S., C.M., M.B., A.B., C.G., D.N., and A.M. edited and revised manuscript; E.S., C.M., M.B., A.B., C.G., D.N., and A.M. approved final version of manuscript.

REFERENCES

1. **Baylie RL, Brayden JE.** TRPV channels and vascular function. *Acta Physiol (Oxf)* 203: 99–116, 2011. doi:10.1111/j.1748-1716.2010.02217.x.
2. **Behringer EJ, Scallan JP, Jafarnejad M, Castorena-Gonzalez JA, Zawieja SD, Moore JEJ Jr, Davis MJ, Segal SS.** Calcium and electrical dynamics in lymphatic endothelium. *J Physiol* 595: 7347–7368, 2017. doi:10.1113/JP274842.
3. **Benham CD, Gunthorpe MJ, Davis JB.** TRPV channels as temperature sensors. *Cell Calcium* 33: 479–487, 2003. doi:10.1016/S0143-4160(03)00063-0.
4. **Bistoletti M, Caputi V, Baranzini N, Marchesi N, Filpa V, Marsilio I, Cerantola S, Terova G, Baj A, Grimaldi A, Pascale A, Frigo G, Crema F, Giron MC, Giaroni C.** Antibiotic treatment-induced dysbiosis differently affects BDNF and TrkB expression in the brain and in the gut of juvenile mice. *PLoS One* 14: e0212856, 2019. doi:10.1371/journal.pone.0212856.
5. **Breslin JW.** Mechanical forces and lymphatic transport. *Microvasc Res* 96: 46–54, 2014. doi:10.1016/j.mvr.2014.07.013.
6. **Breslin JW, Yang Y, Scallan JP, Sweat RS, Adderley SP, Murfee WL.** Lymphatic vessel network structure and physiology. *Compr Physiol* 9: 207–299, 2018. doi:10.1002/cphy.c180015.
7. **Bridenbaugh EA, Gashev AA, Zawieja DC.** Lymphatic muscle: a review of contractile function. *Lymphat Res Biol* 1: 147–158, 2003. doi:10.1089/153968503321642633.
8. **Caires R, Sierra-Valdez FJ, Millet JRM, Herwig JD, Roan E, Vásquez V, Cordero-Morales JF.** Omega-3 fatty acids modulate TRPV4 function through plasma membrane remodeling. *Cell Reports* 21: 246–258, 2017. doi:10.1016/j.celrep.2017.09.029.
9. **Cao DS, Yu SQ, Premkumar LS.** Modulation of transient receptor potential Vanilloid 4-mediated membrane currents and synaptic transmission by protein kinase C. *Mol Pain* 5: 5, 2009. doi:10.1186/1744-8069-5-5.
10. **Caterina MJ, Rosen TA, Tominaga M, Brake AJ, Julius D.** A capsaicin-receptor homologue with a high threshold for noxious heat. *Nature* 398: 436–441, 1999. doi:10.1038/18906.
11. **Clapham DE, Miller C.** A thermodynamic framework for understanding temperature sensing by transient receptor potential (TRP) channels. *Proc Natl Acad Sci USA* 108: 19492–19497, 2011. doi:10.1073/pnas.1117485108.

11a. **Cold Spring Harbor Laboratory Press.** *HEPES-buffered Tyrode's solution* (Online). *Cold Spring Harb*. http://cshprotocols.cshlp.org/content/2007/2/pdb.rec10805.full?sid=8aa05270-7e59-4504-bd64-6636cc504a56. doi:10.1101/pdb.rec10805.

12. **Dhaka A, Viswanath V, Patapoutian A.** Trp ion channels and temperature sensation. *Annu Rev Neurosci* 29: 135–161, 2006. doi:10.1146/annurev.neuro.29.051605.112958.
13. **Everaerts W, Zhen X, Ghosh D, Vriens J, Gevaert T, Gilbert JP, Hayward NJ, McNamara CR, Xue F, Moran MM, Strassmaier T, Uykal E, Owsianik G, Vennekens R, De Ridder D, Nilius B, Fanger CM, Voets T.** Inhibition of the cation channel TRPV4 improves bladder function in mice and rats with cyclophosphamide-induced cystitis. *Proc Natl Acad Sci USA* 107: 19084–19089, 2010. doi:10.1073/pnas.1005333107.
14. **Fischer MJ, Uchida S, Messlinger K.** Measurement of meningeal blood vessel diameter in vivo with a plug-in for ImageJ. *Microvasc Res* 80: 258–266, 2010. doi:10.1016/j.mvr.2010.04.004.
15. **Grimaldi A, Moriondo A, Sciacca L, Guidali ML, Tettamanti G, Negrini D.** Functional arrangement of rat diaphragmatic initial lymphatic network. *Am J Physiol Heart Circ Physiol* 291: H876–H885, 2006. doi:10.1152/ajpheart.01276.2005.
16. **Hille B.** *Ion Channels of Excitable Membranes*. Sunderland, MA: Sinauer Associates, 2001.
17. **Holzer P, Izzo AA.** The pharmacology of TRP channels. *Br J Pharmacol* 171: 2469–2473, 2014. doi:10.1111/bph.12723.
18. **Ito E, Ikemoto Y, Yoshioka T.** Thermodynamic implications of high Q 10 of thermo-TRP channels in living cells. *Biophysics (Nagoya-Shi)* 11: 33–38, 2015. doi:10.2142/biophysics.11.33.
19. **McCloskey KD, Toland HM, Hollywood MA, Thornbury KD, McHale NG.** Hyperpolarisation-activated inward current in isolated sheep mesenteric lymphatic smooth muscle. *J Physiol* 521: 201–211, 1999. doi:10.1111/j.1469-7793.1999.00201.x.

20. **Moorwood C, Liu M, Tian Z, Barton ER.** Isometric and eccentric force generation assessment of skeletal muscles isolated from murine models of muscular dystrophies. *J Vis Exp*: e50036, 2013. doi:10.3791/50036.
21. **Moriondo A, Bianchin F, Marcozzi C, Negrini D.** Kinetics of fluid flux in the rat diaphragmatic submesothelial lymphatic lacunae. *Am J Physiol Heart Circ Physiol* 295: H1182–H1190, 2008. doi:10.1152/ajpheart.00369.2008.
22. **Moriondo A, Boschetti F, Bianchin F, Lattanzio S, Marcozzi C, Negrini D.** Tissue contribution to the mechanical features of diaphragmatic initial lymphatics. *J Physiol* 588: 3957–3969, 2010. doi:10.1113/jphysiol.2010.196204.
23. **Moriondo A, Grimaldi A, Sciacca L, Guidali ML, Marcozzi C, Negrini D.** Regional recruitment of rat diaphragmatic lymphatics in response to increased pleural or peritoneal fluid load. *J Physiol* 579: 835–847, 2007. doi:10.1113/jphysiol.2006.127126.
24. **Moriondo A, Mukenge S, Negrini D.** Transmural pressure in rat initial subpleural lymphatics during spontaneous or mechanical ventilation. *Am J Physiol Heart Circ Physiol* 289: H263–H269, 2005. doi:10.1152/ajpheart.00060.2005.
25. **Moriondo A, Solari E, Marcozzi C, Negrini D.** Spontaneous activity in peripheral diaphragmatic lymphatic loops. *Am J Physiol Heart Circ Physiol* 305: H987–H995, 2013. doi:10.1152/ajpheart.00418.2013.
26. **Moriondo A, Solari E, Marcozzi C, Negrini D.** Diaphragmatic lymphatic vessel behavior during local skeletal muscle contraction. *Am J Physiol Heart Circ Physiol* 308: H193–H205, 2015. doi:10.1152/ajpheart.00701.2014.
27. **Moriondo A, Solari E, Marcozzi C, Negrini D.** Lymph flow pattern in pleural diaphragmatic lymphatics during intrinsic and extrinsic isotonic contraction. *Am J Physiol Heart Circ Physiol* 310: H60–H70, 2016. doi:10.1152/ajpheart.00640.2015.
28. **Muthuchamy M, Zawieja D.** Molecular regulation of lymphatic contractility. *Ann NY Acad Sci* 1131: 89–99, 2008. doi:10.1196/annals.1413.008.
29. **Negrini D, Marcozzi C, Solari E, Bossi E, Cinquetti R, Reguzzoni M, Moriondo A.** Hyperpolarization-activated cyclic nucleotide-gated channels in peripheral diaphragmatic lymphatics. *Am J Physiol Heart Circ Physiol* 311: H892–H903, 2016. doi:10.1152/ajpheart.00193.2016.
30. **Negrini D, Moriondo A.** Lymphatic anatomy and biomechanics. *J Physiol* 589: 2927–2934, 2011. doi:10.1113/jphysiol.2011.206672.
31. **Negrini D, Moriondo A.** Pleural function and lymphatics. *Acta Physiol (Oxf)* 207: 244–259, 2013. doi:10.1111/apha.12016.
32. **Negrini D, Moriondo A, Mukenge S.** Transmural pressure during cardiogenic oscillations in rodent diaphragmatic lymphatic vessels. *Lymphat Res Biol* 2: 69–81, 2004. doi:10.1089/lrb.2004.2.69.
33. **Nybo L, Rasmussen P, Sawka MN.** Performance in the heat-physiological factors of importance for hyperthermia-induced fatigue. *Compr Physiol* 4: 657–689, 2014. doi:10.1002/cphy.c130012.
34. **Poole S, Stephenson JD.** Body temperature regulation and thermoneutrality in rats. *Q J Exp Physiol Cogn Med Sci* 62: 143–149, 1977. doi:10.1113/expphysiol.1977.sp002384.
35. **Scallan JP, Zawieja SD, Castorena-Gonzalez JA, Davis MJ.** Lymphatic pumping: mechanics, mechanisms and malfunction. *J Physiol* 594: 5749–5768, 2016. doi:10.1113/JP272088.
36. **Schmid-Schönbein GW.** Mechanisms causing initial lymphatics to expand and compress to promote lymph flow. *Arch Histol Cytol* 53, *Suppl*: 107–114, 1990. doi:10.1679/aohc.53.Suppl_107.
37. **Schmid-Schönbein GW.** Microlymphatics and lymph flow. *Physiol Rev* 70: 987–1028, 1990. doi:10.1152/physrev.1990.70.4.987.
38. **Schneider CA, Rasband WS, Eliceiri KW.** NIH Image to ImageJ: 25 years of image analysis. *Nat Methods* 9: 671–675, 2012. doi:10.1038/nmeth.2089.
39. **Severinsen T, Munch IC.** Body core temperature during food restriction in rats. *Acta Physiol Scand* 165: 299–305, 1999. doi:10.1046/j.1365-201x.1999.00488.x.
40. **Shavit-Stein E, Artan-Furman A, Feingold E, Ben Shimon M, Itzekson-Hayosh Z, Chapman J, Vlachos A, Maggio N.** Protease activated receptor 2 (PAR2) induces long-term depression in the hippocampus through transient receptor potential vanilloid 4 (TRPV4). *Front Mol Neurosci* 10: 42, 2017. doi:10.3389/fnmol.2017.00042.
41. **Solari E, Marcozzi C, Bartolini B, Viola M, Negrini D, Moriondo A.** Acute exposure of collecting lymphatic vessels to low-density lipoproteins increases both contraction frequency and lymph flow: an in vivo mechanical insight. *Lymphat Res Biol* 18: 146–155, 2020. doi:10.1089/lrb.2019.0040.
42. **Solari E, Marcozzi C, Negrini D, Moriondo A.** Temperature-dependent modulation of regional lymphatic contraction frequency and flow. *Am J Physiol Heart Circ Physiol* 313: H879–H889, 2017. doi:10.1152/ajpheart.00267.2017.
43. **Solari E, Marcozzi C, Negrini D, Moriondo A.** Fluid osmolarity acutely and differentially modulates lymphatic vessels intrinsic contractions and lymph flow. *Front Physiol* 9: 871, 2018. doi:10.3389/fphys.2018.00871.
44. **Taylor JL, Amann M, Duchateau J, Meeusen R, Rice CL.** Neural contributions to muscle fatigue: from the brain to the muscle and back again. *Med Sci Sports Exerc* 48: 2294–2306, 2016. doi:10.1249/MSS.0000000000000923.
45. **Thorneloe KS, Sulpizio AC, Lin Z, Figueroa DJ, Clouse AK, McCafferty GP, Chendrimada TP, Lashinger ES, Gordon E, Evans L, Misajet BA, Demarini DJ, Nation JH, Casillas LN, Marquis RW, Votta BJ, Sheardown SA, Xu X, Brooks DP, Laping NJ, Westfall TD.** N-((1*S*)-1-{[4-((2*S*)-2-{[(2,4-dichlorophenyl)sulfonyl]amino}-3-hydroxypropanoyl)-1 -piperazinyl]carbonyl}-3-methylbutyl)-1-benzothiophene-2-carboxamide (GSK1016790A), a novel and potent transient receptor potential vanilloid 4 channel agonist induces urina. *J Pharmacol Exp Ther* 326: 432–442, 2008. doi:10.1124/jpet.108.139295.
46. **Trangmar SJ, González-Alonso J.** Heat, hydration and the human brain, heart and skeletal muscles. *Sports Med* 49, *Suppl* 1: 69–85, 2019. doi:10.1007/s40279-018-1033-y.
47. **Van Helden DF.** Pacemaker potentials in lymphatic smooth muscle of the guinea-pig mesentery. *J Physiol* 471: 465–479, 1993. doi:10.1113/jphysiol.1993.sp019910.
48. **Vennekens R, Owsianik G, Nilius B.** Vanilloid transient receptor potential cation channels: an overview. *Curr Pharm Des* 14: 18–31, 2008. doi:10.2174/138161208783330763.
49. **von der Weid PY.** Lymphatic vessel pumping. *Adv Exp Med Biol* 1124: 357–377, 2019. doi:10.1007/978-981-13-5895-1_15.
50. **von der Weid PY, Rahman M, Imtiaz MS, van Helden DF.** Spontaneous transient depolarizations in lymphatic vessels of the guinea pig mesentery: pharmacology and implication for spontaneous contractility. *Am J Physiol Heart Circ Physiol* 295: H1989–H2000, 2008. doi:10.1152/ajpheart.00007.2008.
51. **von der Weid PY, Zawieja DC.** Lymphatic smooth muscle: the motor unit of lymph drainage. *Int J Biochem Cell Biol* 36: 1147–1153, 2004. doi:10.1016/j.biocel.2003.12.008.
52. **Watanabe H, Vriens J, Suh SH, Benham CD, Droogmans G, Nilius B.** Heat-evoked activation of TRPV4 channels in a HEK293 cell expression system and in native mouse aorta endothelial cells. *J Biol Chem* 277: 47044–47051, 2002. doi:10.1074/jbc.M208277200.
53. **Wiig H, Swartz MA.** Interstitial fluid and lymph formation and transport: physiological regulation and roles in inflammation and cancer. *Physiol Rev* 92: 1005–1060, 2012. doi:10.1152/physrev.00037.2011.
54. **Xu H, Ramsey IS, Kotecha SA, Moran MM, Chong JA, Lawson D, Ge P, Lilly J, Silos-Santiago I, Xie Y, DiStefano PS, Curtis R, Clapham DE.** TRPV3 is a calcium-permeable temperature-sensitive cation channel. *Nature* 418: 181–186, 2002. doi:10.1038/nature00882.
55. **Zawieja DC.** Contractile physiology of lymphatics. *Lymphat Res Biol* 7: 87–96, 2009. doi:10.1089/lrb.2009.0007.